ELSEVIER

Applied Surface Science 130–132 (1998) 47–53

applied surface science

Diffraction from small antiphase domains: α-$\sqrt{3} \times \sqrt{3}$, β-$\sqrt{3} \times \sqrt{3}$, 6×6 phases of Au adsorbed Si(111)

T. Nagao [a,b,*], C. Voges [b], H. Pfnuer [b], M. Henzler [b], S. Ino [a,1], F. Shimokoshi [a], S. Hasegawa [a,c]

[a] *Department of Physics, Graduate School of Science, University of Tokyo, 7-3-1 Hongo, Bunkyo-Ku, Tokyo 113, Japan*
[b] *Institut fuer Festkoeorperphysik, Universitaet Hannover, Appelstrasse 2, D-30167 Hannover, Germany*
[c] *Core Research and Evolutional Science and Technology, Japan Science and Technology, Japan*

Received 17 September 1997; accepted 10 November 1997

Abstract

Correlation between domain-wall configurations and electron diffraction patterns of the Au-adsorbed Si(111) surface was studied by scanning tunneling microscopy (STM), reflection-high-energy electron diffraction (RHEED), and low-energy electron diffraction (LEED) as a function of Au coverage. Streaks and rings around superreflections in α-$\sqrt{3} \times \sqrt{3}$ (LEED) patterns reflect the zigzagging feature and average size of the small $\sqrt{3} \times \sqrt{3}$ domains. These fine structures become diffuser and then convert to the β-$\sqrt{3} \times \sqrt{3}$ pattern in a continuous way with the increase of Au coverage. This evolution in the diffraction pattern is explained in terms of domain size contraction to a minimum size equivalent to six times of the substrate unit mesh. These smallest domains with dense antiphase domain walls in the β-$\sqrt{3} \times \sqrt{3}$ phase transform to the 6×6 phase by annealing around 600 K, where the smallest domains arrange in a long-range order. This structure transformation may be expressed as 'recrystallization' in the arrangement of small antiphase $\sqrt{3} \times \sqrt{3}$ domains.

PACS: 61.14.Dc; 61.16.Ch; 68.35.Rh; 68.90.+g

Keywords: STM; RHEED; LEED; Antiphase domains; Phase transition; Au, Si(111)

1. Introduction

The Au adsorbed Si(111) surface is one of the most extensively investigated systems among semiconductor surfaces with foreign atom adsorptions. In contrast to many other metal-induced superstructures on Si(111), Au/Si(111) contains significant amounts of disorders as essential structural elements. For example, bright protrusions distributed in a peculiar way in the STM images of the 5×2 phase correspond to streaks in the 5×2 pattern of reflection-high-energy electron diffraction (RHEED) and low-energy electron diffraction (LEED) [1,2]. Zigzagging domain walls in α-$\sqrt{3} \times \sqrt{3}$ phase, which were assumed to correspond to satellites in LEED and streaks in RHEED, were also observed by STM [3–5]. Some inconsistent results concerning satura-

* Corresponding author: Tel.: +81-3-5800-3329; fax: +81-3-5800-3329; e-mail: nagao@phys.s.u-tokyo.ac.jp

[1] Present address: Faculty of Engineering, Utsunomiya University, 2573 Ishii-cho, Utsunomiya, Tochigi 321, Japan.

0169-4332/98/$19.00
PII S0169-4332(98)00023-3

tion Au coverages and atomic structures of these phases are probably attributed to the complexity induced by these disordered structural elements. But, these structural elements, for example, domain walls in the $\sqrt{3} \times \sqrt{3}$ phases, are very interesting since they seem to play an essential role in the variegated structure transitions of this system.

In this study, we report the correlation between zigzagging domain walls in STM images and fine structures in diffraction patterns. The evolution in the diffraction pattern from α-$\sqrt{3} \times \sqrt{3}$ to β-$\sqrt{3} \times \sqrt{3}$ phases, which takes place at Au coverages from $\Theta = 0.76$ to $\Theta = 0.96$, is understood in terms of change in average size of the $\sqrt{3} \times \sqrt{3}$ domains. Above $\Theta = 0.96$, partially ordered β-$\sqrt{3} \times \sqrt{3}$ phase converts to a well-ordered 6×6 phase by annealing around 600 K. The difference between these structures is, as it were, 'amorphous' and 'crystalline' structures by regarding the smallest $\sqrt{3} \times \sqrt{3}$ domains as structural units.

2. Experiments

Experiments were done in a RHEED–STM chamber (UNISOKU model USM501; 5×10^{-9} Pa base pressure), and a SPA–LEED (spot profile analyzing LEED) chamber (4×10^{-9} Pa base pressure) equipped with a cylindrical mirror analyzer and a quartz thickness monitor. The specimen was cut from highly oriented Si wafers with less than 0.1° misorientation from the (111) face. The surface was cleaned by several flash heatings up to 1450 K with a current fed through the Si wafer, followed by

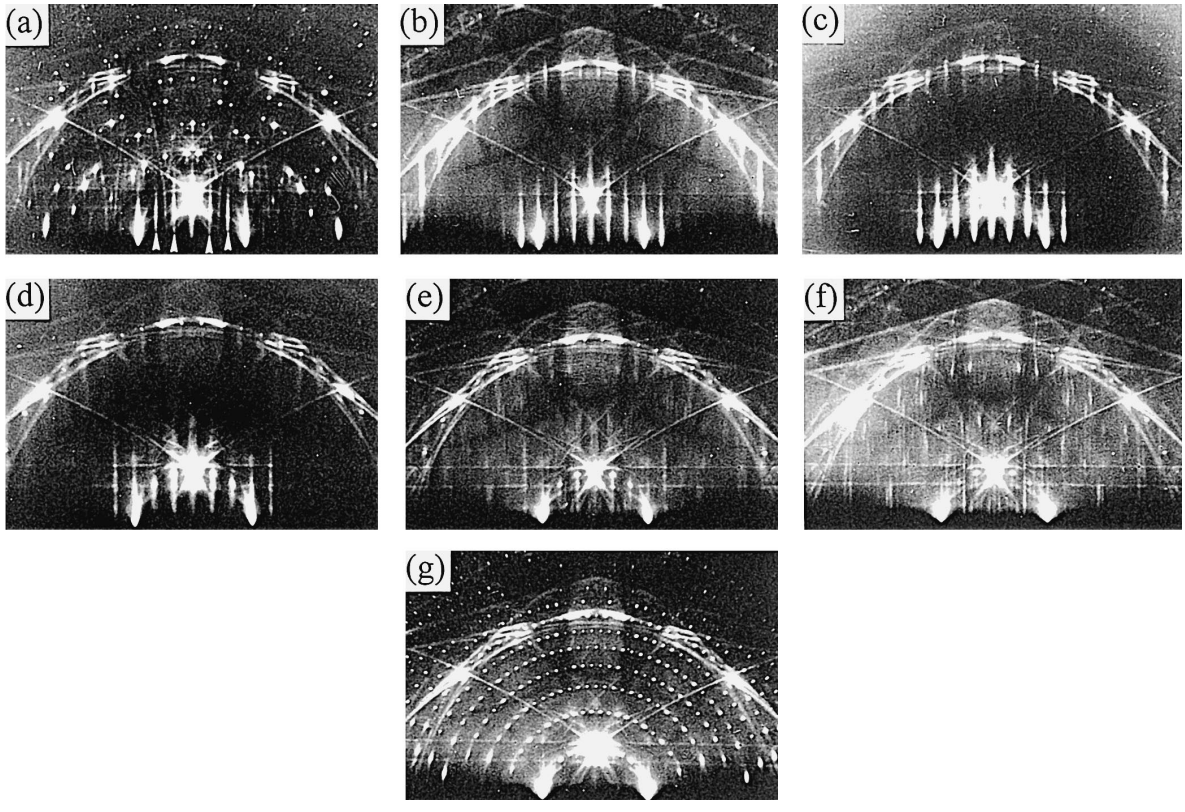

Fig. 1. Evolution of RHEED pattern of the Au adsorbed Si(111) surface as a function Au of coverage Θ. (a) Around $\Theta = 0.65$ (5×2 and (α-$\sqrt{3} \times \sqrt{3}$ phases). White arrowheads indicate the positions of $\sqrt{3} \times \sqrt{3}$ superreflections. (b) At $\Theta = 0.76$ (α-$\sqrt{3} \times \sqrt{3}$). (c) At $\Theta = 0.80$ (α-$\sqrt{3} \times \sqrt{3}$). (d) ($\Theta = 0.85$. (e) $\Theta = 0.90$. (f) $\Theta = 0.96$ (β-$\sqrt{3} \times \sqrt{3}$). (g) $\Theta = 1.0$ (6×6). Electron beam with 15 keV acceleration energy in [11$\bar{2}$] incidence was used.

moderate cooling. In the RHEED–STM observations, Au coverage Θ (expressed by the ratio of the Au atom density to the Si atom density in truncated Si(111) plane) was determined by the duration time in deposition calibrated to the onset of the pure α-$\sqrt{3} \times \sqrt{3}$ pattern; which was previously determined to be $\Theta = 0.76$ by Rutherford backscattering [6]. The determined coverage for each structure agrees well with other ion-scattering spectroscopic measurements [7–9]. Gold was evaporated from a tungsten basket or an alumina-coated tungsten basket keeping the pressure below 2×10^{-7} Pa. In the SPA–LEED experiments, the coverage was determined by a quartz thickness monitor which was also calibrated to the onset of the pure α-$\sqrt{3} \times \sqrt{3}$ pattern. Precision of these coverage determinations was ± 0.02.

3. Results

Fig. 1 shows RHEED patterns taken as a function of Au coverage. Each surface was annealed around 1000 K during deposition and then slowly cooled to room temperature (RT). From $\Theta = 0.55$ to 0.76, 5×2 and α-$\sqrt{3} \times \sqrt{3}$ patterns are mixed (Fig. 1a). At $\Theta = 0.76$, the 5×2 pattern disappears completely and streaky superreflections of α-$\sqrt{3} \times \sqrt{3}$ pattern become brightest (Fig. 1b). As the Au coverage increases, the $\sqrt{3} \times \sqrt{3}$ streaks become diffuser and weaker while the sharp spots become prominent exactly at $\sqrt{3} \times \sqrt{3}$ positions (Fig. 1c–e). The streaks become weakest at $\Theta = 0.90$ (Fig. 1e) and their feature becomes close to that of the β-$\sqrt{3} \times \sqrt{3}$ pattern. At $\Theta = 0.96$, these fine reflections become sharpest as shown in Fig. 1f, which is the definition of the β-$\sqrt{3} \times \sqrt{3}$ pattern. The evolution in RHEED pattern stops at this coverage and no further change is observed at higher coverages. The transition from Fig. 1b to f is continuous; thus, the names of α and β are nominal ones which express the difference at the two extremes at $\Theta = 0.76$ and 0.96. In contrast to streaky and complicated faint reflections in Fig. 1a–f, Fig. 1g shows a sharp 6×6 pattern with a complete long-range order. The sharp 6×6 pattern is formed by annealing the sample at around 600 K during the deposition of very slight amount of Au onto the β-

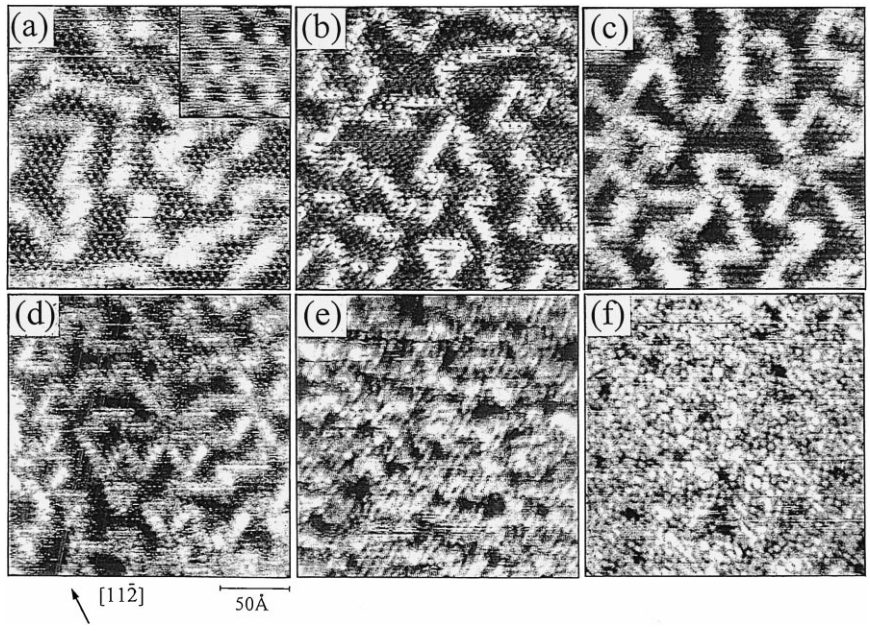

Fig. 2. 200 Å $\times$ 200 Å room temperature STM images taken in a sequence of Au deposition. (a) At $\Theta = 0.76$ (corresponds to(α-$\sqrt{3} \times \sqrt{3}$ pattern). (b) At $\Theta = 0.78$. (c) At $\Theta = 0.80$. (d) At $\Theta = 0.83$. (e) At $\Theta = 0.90$. (f) At $\Theta = 0.96$ (corresponds to β-$\sqrt{3} \times \sqrt{3}$ pattern). Domain boundaries are recognized as zigzagging bright features. All the images were taken at topographic mode with a tip bias of -1.0 V and a tunneling current of 0.4 nA. Inset shows 20 Å $\times$ 20 Å image inside a $\sqrt{3} \times \sqrt{3}$ domain.

$\sqrt{3} \times \sqrt{3}$ phase. The 6×6 pattern is also formed by annealing the β-$\sqrt{3} \times \sqrt{3}$ surface around 600 K without Au deposition, but it requires longer annealing time (more than a few minutes) and the sharpness of the pattern is often degraded. Also, Au coverage required for the 6×6 structure formation is often higher than in the former method.

Fig. 2 shows STM images taken in a sequence of Au deposition. White zigzagging domain walls separate the commensurate $\sqrt{3} \times \sqrt{3}$ domains with displacement vectors equivalent to the primitive translational vectors of the substrate 1×1 mesh. Increase in the domain wall density as a function of Au coverage indicates that the domain walls are heavy or superheavy type, i.e., the domain walls contain more Au atoms than in the $\sqrt{3} \times \sqrt{3}$ domains. From the least-square fit to the domain-wall area fractions versus Au coverage plot obtained from 500 Å $\times$ 500 Å images taken in the same sequence as Fig. 2a–f, local coverages in the commensurate $\sqrt{3} \times \sqrt{3}$ region and the domain-wall region are determined as $\Theta = 0.63 \pm 0.03$ and 1.00 ± 0.03, respectively. From Fig. 2b and d, the actual width of the domain walls seems to be, to the utmost, around 2**a** (**a** corresponds to the primitive translational vector of the substrate 1×1 mesh). We assume that the local atomic structure in the domain wall is Au trimer structure or an analogous one which has the Au coverage of $\Theta = 1.0$. This is because, as we will discuss later, most of the structure analyses that proposed Au trimer model seem to be done close to the coverage of β-$\sqrt{3} \times \sqrt{3}$ where the domain-wall density is very high.

Preferential wall alignment in $[11\bar{2}]$ type directions and inflection angle of 60[4] are the characteristic features clearly seen from the STM images. These results were already reported by previous STM works by Nogami et al. [5], Takami et al. [10], and Falta et al. [11]. What newly discussed in the present study is the behavior from $\Theta = 0.90$ to $\Theta = 0.96$, where the diffraction gradually forms the character of β-$\sqrt{3} \times \sqrt{3}$ pattern. In contrast to the 'sharp $\sqrt{3} \times \sqrt{3}$' spots in the diffraction patterns (Fig. 1e, f), it is quite puzzling that the STM images show highest complexity due to densely packed domain walls (Fig. 2e, f). Since the transition in the diffraction pattern is continuous as shown in Fig. 1b to f, it is also natural to assume that the domain walls are still present at $\Theta = 0.96$ (Fig. 2f) like at lower coverages. However, to see some structural features only from the STM image seems to be hopeless at a glance.

Fourier transformations of STM images can offer some help to extract general structural features in partially ordered systems like the present case. Fig. 3a and b show fast-Fourier transformed (FFT) patterns processed from STM images in wider scans (500 Å $\times$ 500 Å) corresponding to Fig. 2b and Fig. 2f, respectively. Diffuse features as rings and streaks in the FFT patterns are assigned to the domain-wall configuration. It is quite unexpected to see strong and sharp $\sqrt{3} \times \sqrt{3}$ spots in Fig. 3a since the original image just shows small $\sqrt{3} \times \sqrt{3}$ domains (Fig. 2b). It is more perplexing to see sharp $\sqrt{3} \times \sqrt{3}$ spots also in Fig. 3b which is processed from an almost featureless image of Fig. 3f. However, these

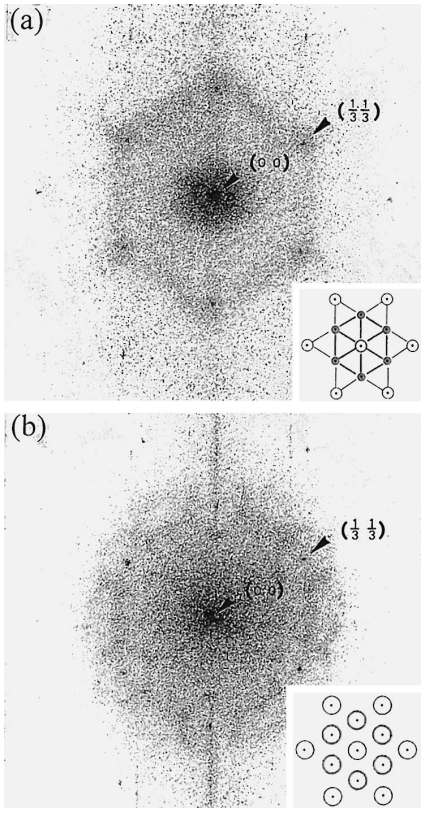

Fig. 3. (a) A fast Fourier transformed (FFT) pattern processed from a STM image of wider scan (500 Å $\times$ 500 Å) corresponding to Fig. 2 (b) (α-$\sqrt{3} \times \sqrt{3}$ pattern). (b) An FFT pattern processed from an STM image corresponding to Fig. 2(f) (β-$\sqrt{3} \times \sqrt{3}$). Insets show schematics of the features in the patterns.

results are well consistent with the RHEED observation shown in Fig. 1.

The FFT patterns processed from STM images normally have limitations in signal-to-noise ratio. The same points can be investigated much more precisely by LEED observations. The patterns taken by SPA–LEED with a transfer width of 2000 Å are shown in Fig. 4 as a function of coverage. The sharp $\sqrt{3} \times \sqrt{3}$ spikes are also seen in these figures. The sharp fundamental spikes indicate that the strain in the overlayer is absent or very small. The streaks running between sharp spots in Fig. 4a correspond to scattering from domain walls running in $[11\bar{2}]$ type directions. Ring around (00) spot in the same figure represents the average separation (about 45 Å) between domain walls. Hexagonal feature around the $\sqrt{3} \times \sqrt{3}$ spikes (see the inset) reflects the average domain size and domain shape. These fine features convert to diffuser and weaker ones as shown in Fig. 4b as the coverage increases. In contrast to the intense and sharp $\sqrt{3} \times \sqrt{3}$ spikes, these weak features have been overlooked in many reports. In those works, this pattern was regarded just as a 'sharp $\sqrt{3} \times \sqrt{3}$ pattern'. Thus, many structure analyses by averaging technique preferentially chose this coverage and derived Au trimer model such as CHCT (conjugate honeycomb-chained-trimer) model or MTLTT (missing top layer twisted trimer) model. However, since the domain wall density around this coverage is very high, we regard that these studies have extracted the structure parameters in the domain walls. In this sense, Au trimer model should be the structure model for the domain walls, not for the commensurate $\sqrt{3} \times \sqrt{3}$ regions. At $\Theta = 0.96$ (Fig. 4c), the diffuse features become clearer to form distinct rings around (00) and $(1/3\ 1/3)$ spikes and oval features between them.

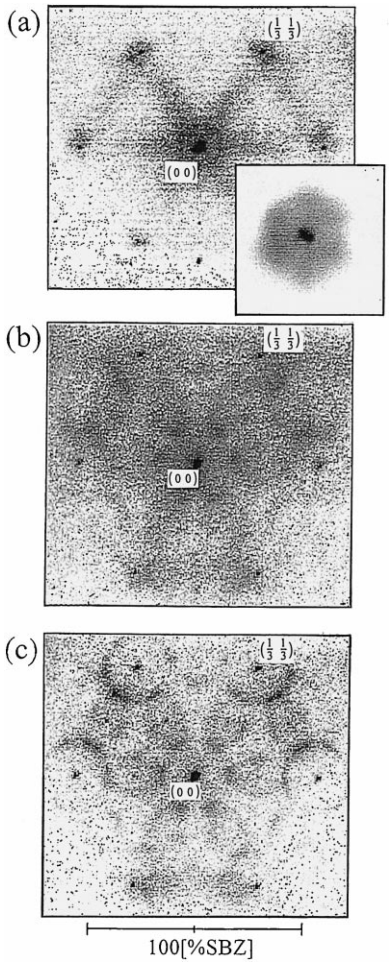

Fig. 4. Evolution of fine structures in LEED patterns as a function of Au coverage at RT. (a) At $\Theta = 0.79$ (α-$\sqrt{3} \times \sqrt{3}$). (b) At $\Theta = 0.92$. (c) $\Theta = 0.96$ (β-$\sqrt{3} \times \sqrt{3}$). Scales are in the units of reduced surface Brillouin zone (SBZ) for Si(111)-1×1.

4. Discussions

Correlation between the electron diffraction patterns and the STM images is unambiguously understood by the above data. The observed continuous evolution in diffraction patterns up to $\Theta = 0.90$ is well understood by the size contraction of the $\sqrt{3} \times \sqrt{3}$ domains seen in STM. However, the question arises whether the domain walls are still present around $\Theta = 0.96$ or not (see Fig. 2f). Answering this question is impossible just by observing this STM image. Observation of diffraction pattern is more useful and reliable. The continuous evolution in diffraction pattern strongly suggests that the structure transformation to β-$\sqrt{3} \times \sqrt{3}$ (from $\Theta = 0.90$ to 0.96) also proceeds in a way similar to the transition from $\Theta = 0.76$ to 0.90, namely, it proceeds by proliferating the (super) heavy domain walls with the Au coverage. Radius of the rings in β-$\sqrt{3} \times \sqrt{3}$

pattern, which is $1/6$ of the unit reciprocal vector, indicates a short-range order of six times of the substrate unit mesh. The most possible assignment to this short-range order is domain size contraction to a minimal size around 6**a**. In order to confirm this idea, we made some simulations. FFT using simplified 2D images imitating some essential features in the STM images, e.g., domain wall alignment in [112] type directions, domain size contraction to 6**a**, reproduces successfully the observed main features in the LEED patterns (Fig. 5). The 2D image in Fig. 5c is created by distributing the minimal sized $\sqrt{3} \times \sqrt{3}$ domains to keep their distances around 6**a**. This result supports the above idea in a visible way. Formation of the long-range ordered 6×6 phase can be explained also by using this model. That is, the small $\sqrt{3} \times \sqrt{3}$ domains rearrange with a translational symmetry with 6**a** periodicity. In this case, this 6×6 structure can be regarded as a crystalline structure made of the smallest $\sqrt{3} \times \sqrt{3}$ domains. It should be noted that the rings in Fig. 5f is not reproduced just by introducing some defects in a 6×6 lattice, e.g., displacing some of the minimal $\sqrt{3} \times \sqrt{3}$ domains from the 6×6 lattice points just enhances background of the sharp 6×6 pattern. Distinct rings appear when the translational symmetry with 6**a** is completely lost, but the distance close to 6**a** is kept among the minimal-sized $\sqrt{3} \times \sqrt{3}$ domains. Thus, the difference between β-$\sqrt{3} \times \sqrt{3}$ and the 6×6 structures can be described, in a sense, as follows: β-$\sqrt{3} \times \sqrt{3}$ is 'amorphous', and 6×6 is 'crystalline' in the arrangement of the smallest antiphase domains of $\sqrt{3} \times \sqrt{3}$, respectively.

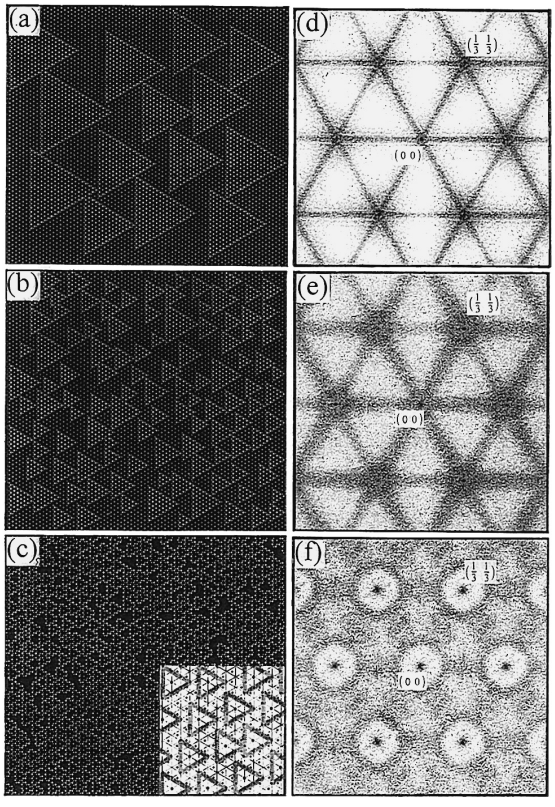

Fig. 5. (a)–(c) Artificially made 2D patterns imitating the characteristic features of STM images. Two out of three sublattices of the different $\sqrt{3} \times \sqrt{3}$ superstructure are shown by differently contrasted regions. (d)–(f) Corresponding FFT patterns processed from the images in the left hand side. Streaks and diffuse features around fundamental and fractional-order spikes become diffuser as the domains become smaller and denser ((d)–(e)). In (c), rings appear around the spikes, whose radius is almost $1/6$ of the fundamental reciprocal vector. Inset in (c) shows the magnified view of densely packed smallest antiphase domains.

Existence of the sharp $\sqrt{3} \times \sqrt{3}$ spots throughout the transition from α-$\sqrt{3} \times \sqrt{3}$ to β-$\sqrt{3} \times \sqrt{3}$ looks puzzling since we see the decrease in domain size in STM images. The sharp spots do not mean large domain size, or long-range order in an ordinary sense. The long-range order here, in this case, arises from the fact that the coherence is kept among the small domains that belong to one type of the sublattices of $\sqrt{3} \times \sqrt{3}$ superstructure. Fig. 5a–c are composed of two types of domains. One type of domains are put in a large domain of another type. The diffraction from the latter large sized domain yields sharp $\sqrt{3} \times \sqrt{3}$ spikes. The interference between the waves diffracted from the two types of domains is not completely destructive, because the phase difference between them is $2\tau/3$. If the domains of three sublattices of the $\sqrt{3} \times \sqrt{3}$ superstructure coexist and their total areas are equivalent, intensities of the $\sqrt{3} \times \sqrt{3}$, spikes are canceled since the waves diffracted from the respective domains interfere destructively. The existence of the $\sqrt{3} \times \sqrt{3}$ spikes in LEED pattern indicates that the ratio among the three types of domains are not equivalent. This discussion is ascertained by the FFT simulation shown in Fig. 5 where the sharp $\sqrt{3} \times \sqrt{3}$ spikes are reproduced by having one type of the $\sqrt{3} \times \sqrt{3}$ domain be absent.

5. Conclusions

Correlation between electron diffraction patterns and STM images of Au-covered Si(111) surface has been studied as a function of Au coverage. Evolution of fine structures in electron diffraction patterns from α-$\sqrt{3} \times \sqrt{3}$ ($\Theta = 0.76$) to β-$\sqrt{3} \times \sqrt{3}$ ($\Theta = 0.96$) pattern has been unambiguously correlated to the decrease in the average domain size. Change in the diffraction pattern takes place in a continuous way, which strongly suggests that the formation of β-$\sqrt{3} \times \sqrt{3}$ structure proceeds by the domain wall packing until their average distance become 6**a**. In spite of a short-range ordered β-$\sqrt{3} \times \sqrt{3}$ structure, a long-range ordered 6×6 phase is formed when the sample is annealed at around 600 K, most effectively during deposition. These two structures can be distinguished, in a sense, as 'amorphous' and 'crystalline' in the $\sqrt{3} \times \sqrt{3}$ domain configuration. Persistence of the sharp $\sqrt{3} \times \sqrt{3}$ spots during the domain size contraction seemed to be perplexing, but has successfully understood as a result of nonuniform area ratio among three types of sublattices of the $\sqrt{3} \times \sqrt{3}$ superstructure within the transfer width in electron diffraction.

Acknowledgements

This work has been supported in part by Grants-in-Aid from the Ministry of education, Science, Culture, and Sports of Japan, especially through the New Frontier Program Grants-in-Aid for Scientific Research (Nos, 08NP1201 and 09NP1201) and the International Scientific Research Program (No. 07044133) conducted by Prof. K. Yagi of Tokyo Institute of Technology. This work has been also supported by the Japan Securities Scholarship Foundation and Nippon Sheet Glass Foundation for Materials Science and Engineering. We also appreciate Dr. H. Tsuru for providing us a useful FFT program.

References

[1] H. Daimon, C. Chung, Y. Watanabe, S. Ino, Surf. Sci. 235 (1990) 142.
[2] A.A. Baski, J. Nogami, C.F. Quate, Phys. Rev. B 41 (1990) 10247.
[3] S. Ino, Reflection high energy electron diffraction and reflection electron imaging of surfaces, in: P.K. Larsen, P.J. Dobson (Eds.), Plenum, (1988): S. Ino, Butsuri, J. Phys. Soc. Japan 37, 82 (1982) (in Japanese).
[4] S. Hasegawa, Y. Nagai, T. Oonishi, S. Ino, Phys. Rev. B 47 (1993) 9903.
[5] J. Nogami, A.A. Baski, C.F. Quate, Phys. Rev. Lett. 65 (1990) 1611.
[6] K. Tsuno, Thesis, University of Tokyo (1990).
[7] J.H. Huang, R.S. Williams, Phys. Rev. B 38 (1988) 4022.
[8] M. Chester, T. Gustafsson, Surf. Sci. 256 (1991) 135.
[9] J. Yuhara, M. Inoue, K. Morita, J. Vac. Sci. Technol. A 10 (2) (1992) 334.
[10] T. Takami, D. Fukushi, T. Nakayama, M. Uda, M. Aono, Jpn. J. Appl. Phys. 33 (1994) 3688.
[11] J. Falta, A. Hille, D. Novikov, G. Materlik, L. Sheehofer, G. Falkenberg, R.L. Johnson, Surf. Sci. 330 (1995) L673.